Magn Reson Med Sci 2020; 19; 141–146
doi:10.2463/mrms.mp.2019-0048
Published Online: June 20, 2019

MAJOR PAPER

Detection of IV-gadolinium Leakage from the Cortical Veins into the CSF Using MR Fingerprinting

Shinji Naganawa[1*], Toshiki Nakane[1], Hisashi Kawai[1], Toshiaki Taoka[1], Hirokazu Kawaguchi[2], Katsuya Maruyama[2], Katsutoshi Murata[2], Gregor Körzdörfer[3,4], Josef Pfeuffer[3], Mathias Nittka[3], and Michihiko Sone[5]

Purpose: It has been reported that leakage of intravenously administered gadolinium-based contrast agents (IV-GBCAs) into the cerebrospinal fluid (CSF) from the cortical veins even in healthy subjects can be detected using a highly sensitive pulse sequence such as heavily T_2-weighted 3D fluid-attenuated inversion recovery and 3D-real inversion recovery (IR). The purpose of this study was to evaluate the feasibility of MR fingerprinting to detect GBCA leakage from the cortical veins after IV-GBCA.

Materials: Fourteen patients with suspected endolymphatic hydrops (EH) who received a single dose of IV-GBCA (39–79 years old) were included. The real IR images as well as MR fingerprinting images were obtained at 4 h after IV-GBCA. T_1 and T_2 values were obtained using MR fingerprinting and analyzed in ROIs covering intense GBCA leakage, and non-leakage areas of the CSF as determined on real IR images. The scan time for real IR imaging was 10 min and that for MR fingerprinting was 41 s.

Results: The mean T_1 value of the ROI in the area of GBCA leakage was 2422 ± 261 ms and that in the non-leakage area was 3851 ± 235 ms ($P < 0.01$). There was no overlap between the T_1 values in the area of GBCA leakage and those in the non-leakage area.

The mean T_2 value in the area of GBCA leakage was 319 ± 90 ms and that in the non-leakage area was 670 ± 166 ms ($P < 0.01$). There was some overlap between the T_2 values in the area of GBCA leakage and those in the non-leakage area.

Conclusion: Leaked GBCA from the cortical veins into the surrounding CSF can be detected using MR fingerprinting obtained in <1 min.

Keywords: *cortical vein, gadolinium, magnetic resonance fingerprinting, magnetic resonance imaging*

Introduction

We have previously reported that intravenously administered gadolinium-based contrast agents (IV-GBCAs) leak into the cerebrospinal fluid (CSF) from the cortical veins even in subjects without blood brain barrier (BBB) disruption.[1–3] This leakage cannot be detected with regular T_1-weighted images, but with heavily T_2-weighted 3D fluid-attenuated inversion recovery (3D-FLAIR) or 3D-real inversion recovery (3D-real IR) images.[4–6] GBCAs in the CSF can enter the brain parenchyma, probably through the perivascular space in humans[1,7–10] as well as animals.[11] This "glymphatic" route is speculated to be the path by which GBCA enters the brain, and ultimately accumulates.[10,12,13] In addition to the cortical veins, the leakage points for GBCAs into the CSF have been suggested to include the peripheral part of the cranial nerves, the circumventricular organs, and the spinal ganglions.[2,14] In our clinical practice, we routinely obtain 3D-real IR images with a longer TR for the evaluation of endolymphatic hydrops (EH) of the inner ear at 4 h after a single dose of IV-GBCA.[5,6] It has been reported that leakage from the cortical vein is not

[1]Department of Radiology, Nagoya University Graduate School of Medicine, 65 Tsurumai-cho, Shouwa-ku, Nagoya, Aichi 466-8550, Japan
[2]Siemens Healthcare KK, Tokyo, Japan
[3]Siemens Healthcare GmbH, Erlangen, Germany
[4]Friedrich-Alexander-Universität Erlangen-Nürnberg, Erlangen, Germany
[5]Department of Otorhinolaryngology, Nagoya University Graduate School of Medicine, Aichi, Japan
*Corresponding author, Phone: +81-52-744-2327, Fax: +81-52-744-2335, E-mail: naganawa@med.nagoya-u.ac.jp

©2019 Japanese Society for Magnetic Resonance in Medicine
This work is licensed under a Creative Commons Attribution-NonCommercial-NoDerivatives International License.

Received: March 28, 2019 | Accepted: May 22, 2019

observed in young subjects below the age of 37 years.[15] The degree of leakage of IV-GBCA into the CSF may be animaging biomarker for the evaluation of aging and neurodegeneration.[15]

Magnetic resonance fingerprinting (MRF) is a method that uses transient signal evolutions and data analysis to simultaneously estimate several quantitative tissue property parameters like T_1 and T_2 relaxation times.[16] Spatial and temporal incoherence through varying acquisition parameters lead to very efficient signal encoding. The acquisition time for one slice of MRF takes 41 s. We now routinely use spiral MRF with fast imaging based on steady-state precession (FISP) to quantify the parameters of various tissues.[17] MRF uses a pseudo-randomized acquisition that causes the signals from different tissues to have a unique evolution or "fingerprint", which is a function of the multiple material properties under investigation. The processing after acquisition involves a pattern-matching algorithm to voxelwise match the fingerprints to a predefined dictionary of simulated signal evolutions featuring different T_1 and T_2 relaxation times. The pattern matching of all voxels leads to quantitative maps of the parameters of interest.[18]

The purpose of this study was to evaluate whether the leakage of IV-GBCA from the cortical veins into the CSF space that is observed by whole-brain 3D-real IR images can be detected by MRF in subjects receiving MR scanning for the evaluation of EH.

Materials and Methods

Patients

Fourteen patients (11 men, 3 women) with suspicion of endolymphatic hydrops were included (age range 39–79 years old, median 63 years). All patients received a single dose (0.1 mmol/kg) of intravenous administration of gadobutrol (Gadovist, Bayer Pharm, Osaka, Japan). They were in the range of older than 37 years, and therefore were expected to have GBCA leakage from the cortical veins.[15]

All patients had an estimated glomerular filtration rate of >60 mL/min/1.73 m^2. Patients received only a single dose (0.1 mmol/kg) of intravenously administered gadobutrol (Gadovist). The ethical committee of our institution approved this study with written consent from the patients.

MRI

The images were obtained on a 3T MR scanner (MAGNETOM Skyra, Siemens Healthcare, Erlangen, Germany) using a 32-channel array head coil at 4 h after IV-GBCA.

Axial-slab 3D-real IR images covering the whole brain were obtained over 10 min. The axial slab was set parallel to the anterior commissure-posterior commissure (AC–PC) line. The slice thickness was 1 mm. Scan parameter details are shown in Table 1.

Table 1 Pulse sequence parameters

Sequence name	Type	Repetition time (ms)	Echo time (ms)	Inversion time (ms)	Flip angle (°)	Section thickness/ gap (mm)	Pixel size (mm)	Number of slices	Echo train length	Field of view (mm)	Matrix size	Number of excitations	Scan time (min)
3D-real IR	SPACE with inversion pulse	15130	549	2700	90/ constant 145	1/0	0.5 × 0.5	256	256	165 × 196	324 × 384	1	10

SPACE, sampling perfection with application-optimized contrasts using different flip angle evolutions; 3D-real IR, 3D inversion recovery with phase sensitive reconstruction (real reconstruction).

This sequence utilizes a frequency selective fat suppression pre-pulse, non-slab selective excitation pulse, and non-slab selective inversion pulse.

3D slab is set in an axial orientation.

MR fingerprinting

The pulse sequence for 2D-MRF, based on FISP, uses a spiral readout trajectory, inversion recovery pulse, variable TR, and variable flip angles. The slice thickness for this acquisition was 5 mm and had a square FOV of 300 mm. The matrix size was 256 × 256. The scan time was 41 s with 3000 echoes for one slice.

The scan parameters included an echo time of 2.0 ms and an inversion time of 20.6 ms. The TR ranged from 12.1 to 15.0 ms, and the flip angle ranged from 0° to 74°. Each echo encoded an image by a single spiral readout with a variable-density *k*-space trajectory (24- to 48-fold undersampling), and the spiral trajectory was rotated by 82.5° for each repetition time to improve the temporal incoherence of the undersampling artifacts.[19,20]

The axial slice location for the MRF scan was selected at 25 mm below the vertex of the cranium. The axial slice was set parallel to the 3D-real IR slab. At this parietal position, it has been reported that leakage from the cortical veins is frequently visible.[15]

To compensate for the inhomogeneity of the RF-field (B_1^+), an automated field correction was applied. Before the actual MRF scan was started, an RF-field-mapping sequence was triggered.[21]

After acquisition of the MRF data, the scanner automatically performed pattern recognition between the calculated dictionary and the measured time course. The dictionary was calculated for a range of discrete T_1, T_2 and B_1^+ values by performing a Bloch simulation over a voxel of 200 spins taking the slice profile into account.[22] A subset was extracted from the dictionary according to the B_1^+ value from the separately measured RF-field-mapping sequence for every voxel. The actual voxelwise matching process then took place in this subset in T_1 and T_2 dimensions. The inner products between the normalized measured time course of each pixel and all entries of the normalized dictionary were calculated, and the dictionary entry corresponding to the maximum value of the inner product was taken to represent the closest signal evolution to the one acquired. The T_1 and T_2 values were then derived from this entry to generate the T_1 and T_2 relaxation maps.[17]

The range and step size of the calculated dictionary for the MRF utilized in this study is shown below:

T_1: range 10–4500 ms.
Step-size: 10 ms (10–100 ms), 20 ms (100–1000 ms), 40 ms (1000–2000 ms) and 100 ms (2050–2950, 3100–4500 ms).
T_2: range 2–3000 ms.
Step-size: 2 ms (2–100 ms), 5 ms (100–150 ms), 10 ms (160–300 ms), 50 ms (300–800 ms), 100 ms (800–1600 ms) and 200 ms (1600–3000 ms).
B_1^+: range 0.60–1.40.
Step-size: 0.01.

Image evaluation

In the 3D-real IR image at 25 mm below the convex, an experienced neuroradiologist (S.N.) placed a circular ROI with a diameter of 3 mm in the CSF area containing GBCA leakage as well as in the CSF area without discernable GBCA leakage. The ROIs were set at least 5 mm away from the inner surface of the skull to reduce partial-volume effects. If there were multiple CSF areas with GBCA leakage, the observer placed the ROI in the most uniform high signal CSF area where the brain parenchyma and vessels could be avoided. To select the position of the CSF area without GBCA leakage, the observer placed the ROI in the most uniformly low-signal CSF area where the brain parenchyma and vessels could be avoided. The images were evaluated on a PACS viewer (RapideyeCore, Canon Medical Systems, Tokyo, Japan). The display condition was set as constant with a window width of 80 and a window level of 10. Then the ROIs were copied and pasted onto the MRF maps.

The T_1, T_2 values and the signal intensity values on 3D-real IR, were compared between the ROIs in the CSF area with GBCA leakage and those without GBCA leakage. An example of the ROI location is shown in Fig. 1. We used 5% as a threshold to determine statistical significance. The software R (version 3.3.2, R Foundation for Statistical Computing, Vienna, Austria, https://www.R-project.org/) was used for statistical analyses.

A paired Student's *t*-test was used for the comparison between the ROIs in the area of GBCA leakage and the non-leakage area in the CSF.

Results

The mean T_1 value of the ROI in the area of GBCA leakage was 2422 ± 261 ms and that in the non-leakage area was 3851 ± 235 ms ($P < 0.01$). There was no overlap between the T_1 values in the area of GBCA leakage and those in the non-leakage area (Fig. 2a).

The mean T_2 value in the area of GBCA leakage was 319 ± 90 ms and that in the non-leakage area was 670 ± 166 ms ($P < 0.01$). There was overlap between the T_2 values in the area of GBCA leakage and those in the non-leakage area (Fig. 2b).

The mean signal intensity value of 3D-real IR in the area of GBCA leakage was 64.4 ± 27.5 and that in the non-leakage area was −46.4 ± 5.3 ($P < 0.01$). There was no overlap between the signal intensity values of 3D-real IR in the area of GBCA leakage and those in the non-leakage area (Fig. 2c).

Discussion

MRF is a rapid quantification method to assess multiple parameters simultaneously. Multiple kinds of quantitative

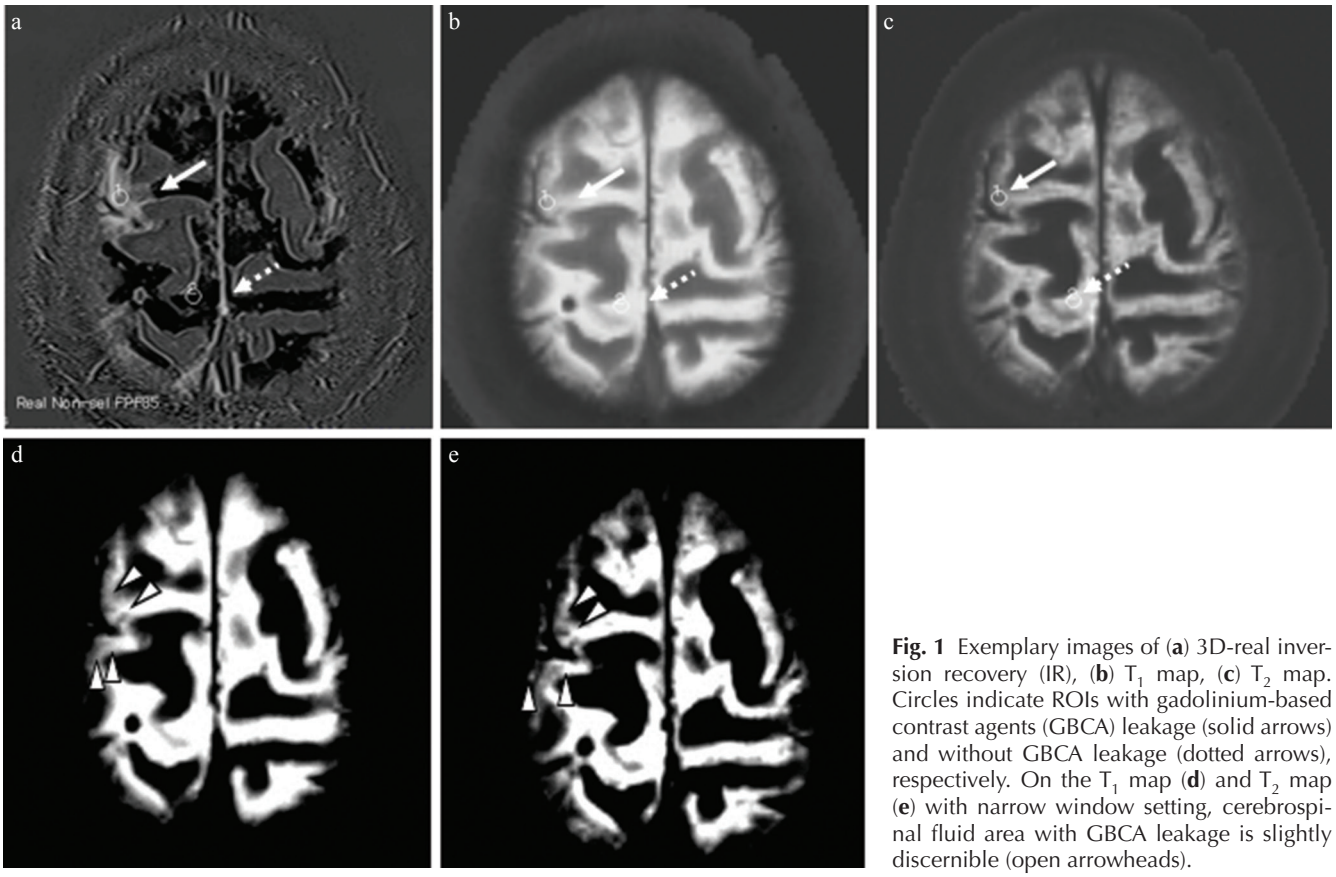

Fig. 1 Exemplary images of (**a**) 3D-real inversion recovery (IR), (**b**) T_1 map, (**c**) T_2 map. Circles indicate ROIs with gadolinium-based contrast agents (GBCA) leakage (solid arrows) and without GBCA leakage (dotted arrows), respectively. On the T_1 map (**d**) and T_2 map (**e**) with narrow window setting, cerebrospinal fluid area with GBCA leakage is slightly discernible (open arrowheads).

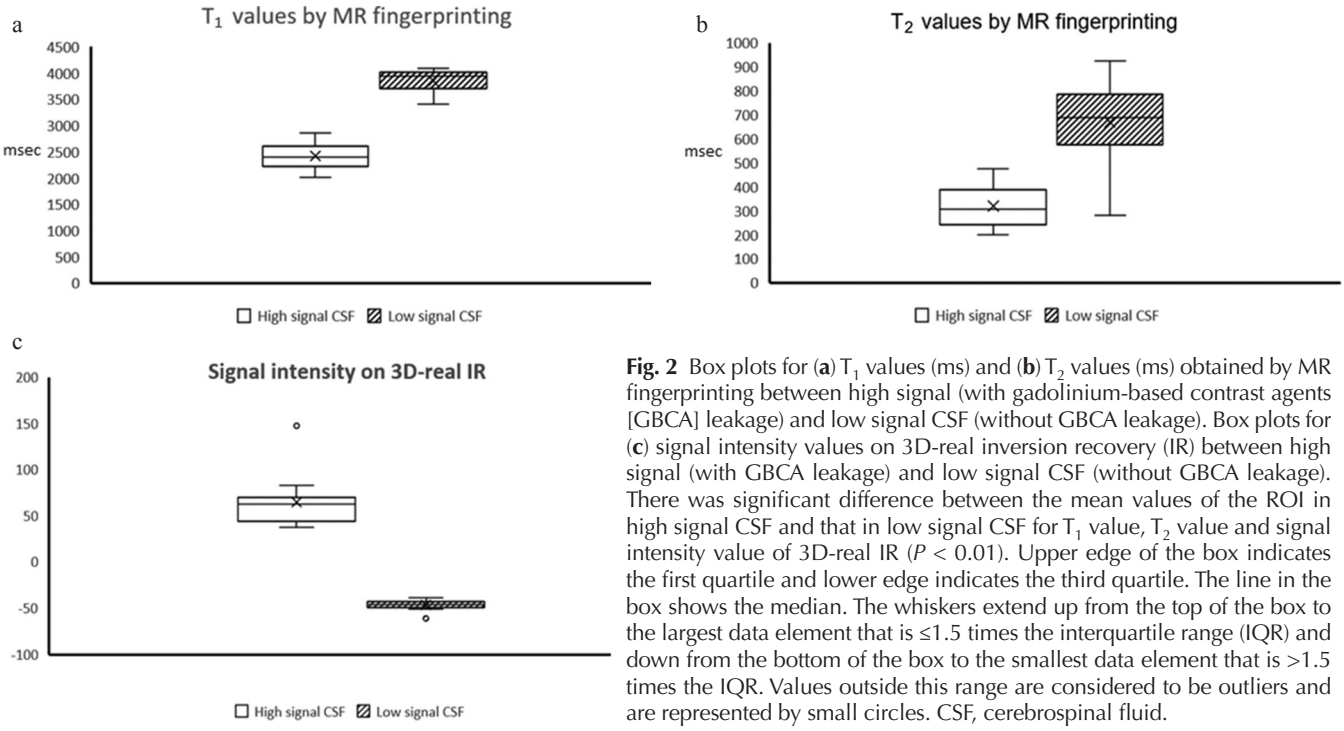

Fig. 2 Box plots for (**a**) T_1 values (ms) and (**b**) T_2 values (ms) obtained by MR fingerprinting between high signal (with gadolinium-based contrast agents [GBCA] leakage) and low signal CSF (without GBCA leakage). Box plots for (**c**) signal intensity values on 3D-real inversion recovery (IR) between high signal (with GBCA leakage) and low signal CSF (without GBCA leakage). There was significant difference between the mean values of the ROI in high signal CSF and that in low signal CSF for T_1 value, T_2 value and signal intensity value of 3D-real IR ($P < 0.01$). Upper edge of the box indicates the first quartile and lower edge indicates the third quartile. The line in the box shows the median. The whiskers extend up from the top of the box to the largest data element that is ≤1.5 times the interquartile range (IQR) and down from the bottom of the box to the smallest data element that is >1.5 times the IQR. Values outside this range are considered to be outliers and are represented by small circles. CSF, cerebrospinal fluid.

data can be obtained without pixel misregistration.[16,17,23] The stability and accuracy of MRF has been reported in phantoms[23] and *in vivo*.[24]

IV-GBCA leaks into the CSF in older subjects.[25–28] This finding may be a part of the normal aging process; however, it also might be a biomarker of neurodegeneration.[15,26,28]

To better understand the importance of GBCA leakage into the CSF from the cortical veins, we need more research. MRF can facilitate studies to further understand this phenomenon due to its brief scan time when we scan the limited number of slices of MRF. With the data from the larger number of subjects, we might be able to correlate the degree of GBCA leakage into the CSF with aging, the status of various diseases, cognitive function and so on. The short acquisition time, quantitative nature and reproducibility allow MR fingerprinting to serve as the valuable tool for the longitudinal studies, especially focused to evaluate the function of glymphatic system.

Heavily T_2-weighted 3D-FLAIR and 3D-real IR images are quite sensitive to low concentrations of GBCA in fluid. However, they are not sensitive to T_1 changes in brain parenchyma.[4–6] The longitudinal magnetization of the brain parenchyma fully recovers relative to CSF after a long inversion time as conventionally used, therefore the presence of GBCA in the brain parenchyma cannot be measured, if these sequences focus on the signal changes inside CSF. In other words, these sequences have a narrow dynamic range to evaluate the differences in T_1. MRF has a wide dynamic range, which is applicable to both brain parenchyma as well as CSF.

This study had some limitations. The number of subjects was small. The evaluation was done with manual placement of small ROIs. We evaluated only post-contrast-enhanced images. We did not evaluate the sensitivity of MRF to very slight CSF enhancement, which can be barely detected by 3D-real IR. Partial-volume effects may affect the T_1 and T_2 values due to the use of a relatively thick slice (5 mm) for MRF. However, we placed the ROI so that it was centered on the area of GBCA leakage into the CSF according to the 3D-real IR image (1 mm). In addition, there could be some CSF flow. While flow effects on MRF have not been clarified, recent studies have indicated that T_2 values are more sensitive than T_1 values to in-plane and especially through-plane motions in 2D FISP–MRF.[29,30] The wider range of T_2 values compared with T_1 values might be caused by motion within the CSF. Therefore, the use of T_1 values to detect GBCA leakage into the CSF rather than T_2 values might be a reasonable strategy. Furthermore, it has been reported, that when using time spatial spin labeling inversion pulse imaging, there is no CSF pulsation or flow in the subarachnoid space over the convexity in the normal brain, nor in the hydrocephalic brain.[31] Therefore, we believe that the CSF movement in the convexity area is too small to cause a significant error in the T_1 value measurement. The other limitation is that the maximum T_1 values of the MRF dictionary (4500 ms) could underestimate the CSF T_1 values over 4500 ms. From the above, further research is needed to assess whether MRF is useful for CSF; however, we could clearly detect GBCA leakage into the CSF. Our result has the potential to extend the clinical applications for MRF.

Conclusion

Leaked GBCA from the cortical veins into the surrounding CSF can be detected using MRF obtained in <1 min.

Conflicts of Interest

Hirokazu Kawaguchi, Katsuya Maruyama, and Katsutoshi Murata are employees of Siemens Healthcare KK. Josef Pfeuffer and Mathias Nittka are employees of Siemens Healthcare GmbH.

The PhD program of Gregor Körzdörfer is funded by Siemens Healthcare GmbH.

The other authors declare that they have no conflicts of interest.

References

1. Naganawa S, Nakane T, Kawai H, Taoka T. Gd-based contrast enhancement of the perivascular spaces in the basal ganglia. Magn Reson Med Sci 2017; 16:61–65.
2. Naganawa S, Suzuki K, Yamazaki M, Sakurai Y. Serial scans in healthy volunteers following intravenous administration of gadoteridol: time course of contrast enhancement in various cranial fluid spaces. Magn Reson Med Sci 2014; 13:7–13.
3. Ohashi T, Naganawa S, Ogawa E, Katagiri T, Kuno K. Signal intensity of the cerebrospinal fluid after intravenous administration of gadolinium-based contrast agents: strong contrast enhancement around the vein of labbe. Magn Reson Med Sci 2019; 18:194–199.
4. Naganawa S, Kawai H, Sone M, Nakashima T. Increased sensitivity to low concentration gadolinium contrast by optimized heavily T2-weighted 3D-FLAIR to visualize endolymphatic space. Magn Reson Med Sci 2010; 9:73–80.
5. Naganawa S, Kawai H, Taoka T, Sone M. Improved HYDROPS: imaging of endolymphatic hydrops after intravenous administration of gadolinium. Magn Reson Med Sci 2017; 16:357–361.
6. Naganawa S, Kawai H, Taoka T, Sone M. Improved 3D-real inversion recovery: a robust imaging technique for endolymphatic hydrops after intravenous administration of gadolinium. Magn Reson Med Sci 2019; 18:105–108.
7. Eide PK, Ringstad G. MRI with intrathecal MRI gadolinium contrast medium administration: a possible method to assess glymphatic function in human brain. Acta Radiol Open 2015; 4:2058460115609635.
8. Eide PK, Ringstad G. Delayed clearance of cerebrospinal fluid tracer from entorhinal cortex in idiopathic normal pressure hydrocephalus: a glymphatic magnetic resonance imaging study. J Cereb Blood Flow Metab 2019; 39: 1355–1368.
9. Eide PK, Vatnehol SAS, Emblem KE, Ringstad G. Magnetic resonance imaging provides evidence of glymphatic drainage from human brain to cervical lymph nodes. Sci Rep 2018; 8:7194.

10. Taoka T, Naganawa S. Gadolinium-based contrast media, cerebrospinal fluid and the glymphatic system: possible mechanisms for the deposition of gadolinium in the brain. Magn Reson Med Sci 2018; 17:111–119.
11. Jost G, Frenzel T, Lohrke J, Lenhard DC, Naganawa S, Pietsch H. Penetration and distribution of gadolinium-based contrast agents into the cerebrospinal fluid in healthy rats: a potential pathway of entry into the brain tissue. Eur Radiol 2017; 27:2877–2885.
12. Taoka T, Jost G, Frenzel T, Naganawa S, Pietsch H. Impact of the glymphatic system on the kinetic and distribution of gadodiamide in the rat brain: observations by dynamic MRI and effect of circadian rhythm on tissue gadolinium concentrations. Invest Radiol 2018; 53:529–534.
13. Taoka T, Masutani Y, Kawai H, et al. Evaluation of glymphatic system activity with the diffusion MR technique: diffusion tensor image analysis along the perivascular space (DTI-ALPS) in Alzheimer's disease cases. Jpn J Radiol 2017; 35:172–178.
14. Naganawa S, Taoka T, Kawai H, Yamazaki M, Suzuki K. Appearance of the organum vasculosum of the lamina terminalis on contrast-enhanced MR imaging. Magn Reson Med Sci 2018; 17:132–137.
15. Naganawa S, Nakane T, Kawai H, Taoka T. Age dependence of gadolinium leakage from the cortical veins into the cerebrospinal fluid assessed with whole brain 3D-real inversion recovery MR imaging. Magn Reson Med Sci 2019; 18:163–169.
16. Ma D, Gulani V, Seiberlich N, et al. Magnetic resonance fingerprinting. Nature 2013; 495:187–192.
17. Jiang Y, Ma D, Seiberlich N, Gulani V, Griswold MA. MR fingerprinting using fast imaging with steady state precession (FISP) with spiral readout. Magn Reson Med 2015; 74:1621–1631.
18. European Society of Radiology (ESR). Magnetic Resonance Fingerprinting - a promising new approach to obtain standardized imaging biomarkers from MRI. Insights Imaging 2015; 6:163–165.
19. Pfeuffer J, Kechagias A, Meyer CH, Körzdörfer G, Nittka M. Mitigation of spiral undersampling artifacts in magnetic resonance fingerprinting (MRF) by adapted interleave reordering. Proceedings of the 25th Annual Meeting of ISMRM, Honolulu, 2017; 0133
20. Körzdörfer G, Kluge T, Pfeuffer, J, et al. Spatial biases in magnetic resonance fingerprinting parameter maps arising from undersampling patterns. Proceedings of the 25th Annual Meeting of ISMRM, Honolulu, 2017; 3956.
21. Chung S, Kim D, Breton E, Axel L. Rapid B_1^+ mapping using a preconditioning RF pulse with TurboFLASH readout. Magn Reson Med 2010; 64:439–446.
22. Ma D, Coppo S, Chen Y, et al. Slice profile and B_1 corrections in 2D magnetic resonance fingerprinting. Magn Reson Med 2017; 78:1781–1789.
23. Jiang Y, Ma D, Keenan KE, Stupic KF, Gulani V, Griswold MA. Repeatability of magnetic resonance fingerprinting T_1 and T_2 estimates assessed using the ISMRM/NIST MRI system phantom. Magn Reson Med 2017; 78:1452–1457.
24. Körzdörfer G, Kirsch R, Liu K, et al. Multicenter and multiscanner reproducibility of magnetic resonance fingerprinting relaxometry in the brain. Proceedings of the 27th Annual Meeting of ISMRM, Paris, 2018; 0798.
25. Berger F, Kubik-Huch RA, Niemann T, et al. Gadolinium distribution in cerebrospinal fluid after administration of a gadolinium-based MR contrast agent in humans. Radiology 2018; 288:703–709.
26. Freeze WM, Schnerr RS, Palm WM, et al. Pericortical enhancement on delayed postgadolinium fluid-attenuated inversion recovery images in normal aging, mild cognitive impairment, and Alzheimer disease. AJNR Am J Neuroradiol 2017; 38:1742–1747.
27. Naganawa S, Yamazaki M, Kawai H, Sone M, Nakashima T. Contrast enhancement of the anterior eye segment and subarachnoid space: detection in the normal state by heavily T_2-weighted 3D FLAIR. Magn Reson Med Sci 2011; 10:193–199.
28. Nehra AK, McDonald RJ, Bluhm AM, et al. Accumulation of gadolinium in human cerebrospinal fluid after gadobutrol-enhanced MR imaging: a prospective observational cohort study. Radiology 2018; 288:416–423.
29. Yu Z, Zhao T, Assländer J, Lattanzi R, Sodickson DK, Cloos MA. Exploring the sensitivity of magnetic resonance fingerprinting to motion. Magn Reson Imaging 2018; 54:241–248.
30. Körzdörfer G, Speier P, Schröter S, et al. Evaluating the influence of motion on FISP–MRF. Proceedings of the 27th Annual Meeting of ISMRM, Paris, 2018; 4085.
31. Yamada S, Kelly E. Cerebrospinal fluid dynamics and the pathophysiology of hydrocephalus: new concepts. Semin Ultrasound CT MR 2016; 37:84–91.